PCCP

Solution vs. gas phase relative stability of the choline/acetylcholine cavitand complexes

Journal:	*Physical Chemistry Chemical Physics*
Manuscript ID:	CP-ART-11-2014-005354.R1
Article Type:	Paper
Date Submitted by the Author:	18-Dec-2014

Complete List of Authors:	ABDOUL-CARIME, Hassan; Université Lyon1, Institut de Physique Nucléaire de Lyon Farizon, Bernadette; University Lyon 1, Farizon, Michel; University Lyon 1, Mulatier, Jean-Christophe; University Lyon 1, Dutasta, Jean-Pierre; University Lyon 1, Chermette, Henry; University Lyon 1,

Solution vs. gas phase relative stability of the choline/acetylcholine cavitand complexes

Hassan ABDOUL-CARIME[1], Bernadette FARIZON[1], Michel FARIZON[1],

[1] Université de Lyon; Université Claude Bernard Lyon1; Institut de Physique Nucléaire de Lyon, CNRS/IN2P3 UMR 5822, 43 Bd du 11 novembre 1918, 69622 Villeurbanne Cedex, France

Jean-Christophe MULATIER[2], Jean-Pierre DUTASTA[2],

[2] Université de Lyon, Laboratoire de Chimie, Institut de Chimie de Lyon, Ecole Normale Supérieure de Lyon, Laboratoire de Chimie, CNRS UMR 5182 , 46 allée d'Italie, 69364 Lyon Cedex 07, France

Henry CHERMETTE[3],

[3] Université de Lyon; Université Claude Bernard Lyon; Institut des Sciences Analytiques, CNRS UMR 5280, 43 boul. 11 novembre, 69622 Villeurbanne Cedex, France

ABSTRACT

How the information obtained from the gas phase experiments can reflect the processes in solution is a crucial question for the analytical chemistry, and particularly the selective host-guest recognition mechanisms which are fundamental in biology. Here we combine the ElectroSpray Ionization mass spectrometry (ESI-MS) and the Collision Induced Dissociation (CID) experiments to the density functional theory to investigate the interaction of the acetylcholine and the choline cation with a triphosphonate cavitand. While the relative abundance of the cation complexes in the ESI mass spectrum reflects the preferential capture of acetylcholine ion over the choline ion by the cavitand in the solution, the gas phase CID measurements indicate that after desolvation the choline cation is the most strongly bound to the host. The experimental results are interpreted by theory that underlines the role of the counterion in the stabilization of the complexes in solution and therefore in the selective recognition of substrates of biological interest.

1. Introduction

Molecular recognition is fundamental in many biological processes **[1]** and particularly important in the transmission of the neuronal information in living systems, where neurotransmitters play an important role. For instance, acetylcholinesterase is an essential enzyme that catalyzes the hydrolysis of acetylcholine to choline implicated in the relaying of the nerve signals **[2]**. It has been shown that the quaternary ammonium head of acetylcholine interacts strongly with aromatic residues of the enzyme close to the catalytic site **[3],** enlightening the importance of the cation-π interactions **[4**,**5**,**6]**. For many decades, chemists aspired to design synthetic receptors that mimic the enzyme machinery, and in the recent literature the differentiation of acetylcholine from choline by synthetic molecular receptors has been reported **[7**,**8]**. A large number of molecular receptors have been designed, which present aromatic molecular cavities. For example, cyclophanes **[9**,**10**,**11]**, calixarenes **[12**,**13**,**14**,**15]** and cryptophanes **[16**,**17**,**18]** are known to form complexes with ammonium guests with high association constants even in aqueous media **[19]**. Similarly, anions such as nitrate can be encapsulated in a selective orientation in receptors, playing a key role in the structure and therefore in chemistry and biochemistry **[20**,**21]**. Finally the bowl shape structure of the phosphonate cavitand hosts is particularly well suited for these charged species and exhibited in several cases high selectivity and chiral discrimination **[22**,**23**,**24**,**25**,**26]**.

To characterize the association of an ammonium guest with a molecular host, NMR and fluorescence spectroscopy or X-ray diffraction studies have been widely used. On the other hand, mass spectrometry has been shown to be a reliable tool for the exploration of host-guest systems **[8,27**,**28**,**29**,**30]** and the determination of thermochemical data **[8, 31**,**32**,**33**,**34]**. For instance the preferential capture of the acethylcholine ions by a 3*i*PO phophonate cavitand (see Fig. 1) has been recently observed by Electrospray Mass

Spectrometry (ESI-MS) and corroborated by NMR experiments **[8]**. ESI is a soft ionization method that transfers ions from fragile or low volatile compounds in solution into the gas phase **[35]**. Combining the ESI to a mass spectrometry technique (MS) and the Collision Induced Dissociation (CID) method can usually provide information on the solution characteristics (solvents, analytes) but also chemical reactions **[36**,**37**,**38**,**39**,**40]**. Nevertheless, it is not clear how far the properties of the ion-molecule interaction extracted from the gas phase ESI-MS-CID technique can reflect that in the solution because of the presence and the nature of the environing solvent and counterions **[41**,**42**,**43]**.

In this contribution, using mass spectrometry technique, we show that the acetylcholine ion (ACh^+) is preferentially captured by the 3*i*PO phosphonato-cavitand **1** in comparison to the choline ion (Ch^+), in agreement with the observations from the chemical analysis methods in solution. In contrast, the gas phase Collision Induced Dissociation experiments indicate that in the gas phase the Ch^+-**1** ion complex is more strongly bound than the ACh^+-**1** ion. The relative stability of the ion complexes in the solution vs. the gas phase can be explained by the effect of the counterion as shown by DFT calculations.

2. Experimental Section

All experiments were carried out with an Electrospray Ionization source combined with a Time-Of-Flight mass spectrometer (ESI-TOF, Z-Spray Ultima, Micromass, UK) operating in the positive ion mode. The samples were continuously sprayed at a 4.5b of the nitrogen drying gas into a differentially pumped region at working pressure of 1.6 mb. The constant injection rate of 15μL/min was controlled by means of a syringe pump (NewEra Syringepump Systems Inc.). The ESI needle was biased at +3000V and a voltage of 100V was applied to the cone. The source and desolvation temperatures were set to 353 K and 423 K, respectively.

The *3i*PO phosphonato-cavitand **1** (Fig. 1) bearing phenethyl substituents at its narrow rim of 1271.286 amu, was synthetized as previously reported **[44]**. Figure 1 shows the structure of the host **1** in comparison to the host **2** which has been investigated earlier **[8]**. Chloroform (spectroscopic grade from Sigma-Aldrich) was used as solvent. The acetylcholine picrate (ACh^+Pic^-) and the choline picrate (Ch^+Pic^-) salts were easily prepared by anion exchange from the ACh^+I^- and Ch^+I^- iodide salts. The picrate salts are only partly dissolved in chloroform and their solubility in this solvent are not known. The used solution of ACh^+Pic^- was obtained by further dilution in chloroform in a ratio of 1:100. A solution of 1.0 μmol/L of host material was obtained at room temperature by diluting 1.0 mg of **1** in chloroform. From this solution, we prepared two solutions (A) and (B). The solution (A) is obtained by adding the host **1**/chloroform to the guest Ch^+Pic^-/chloroform. The number of the Ch^+ ions was verified by mass spectrometry to exceed that of the host (see below, Fig.2A). Thus at equilibrium all **1** molecules are expected to complex with the choline ions. The solution (B) is prepared by adding 1 μL of the ACh^+Pic^-/chloroform solution described above to 1mL of the solution (A).

3. Computational method

DFT calculations were performed with the ADF2010 software **[45**,**46]** at different levels of calculations. This software allows the decomposition of molecules into fragments, which can be atoms or groups of atoms, making the interpretation of results easier, as concepts from qualitative MO theory can be used within the framework of an accurate method. Geometry optimizations were obtained at LDA level (WVN functional **[47]**) with a double zeta basis set, and (small) frozen cores. The geometries of both complexes, including or not the picrate (Pic^-) counterion were optimized. Bonding energies were then calculated with orbitals calculated with PBE functional **[48]** and triple zeta+ polarization (TZP) basis set, and no frozen cores. With the help of the density obtained with these SCF orbitals, bonding

energies were calculated with several exchange-correlation functionals, belonging to GGA, metaGGA, hybrid families; functionals with added ad-hoc dispersion terms were also tested. This is easily done with the keyword "metaGGA" in ADF.

An extensive work has been performed these two last decades to improve exchange-correlation functional beyond the LDA approximation, involving the development of the so-called GGA, metaGGA and hybrid functionals, and more recently, range-separated, double hybrid or dispersion-corrected functionals. Many benchmarks have been performed on specific systems or broad panel of systems, testing specific properties (e.g. spectroscopy or barrier heights) or several properties. These kind of benchmarks let estimate the accuracy provided by each class of functional applied to a general system, and also delivers the important consideration that the relative energy between two similar systems is not so sensitive to the exact geometry of the compared molecules: therefore experimental geometries, as well as geometries optimized at a given (lower) level of theory may be successfully used to perform energy calculations at higher level of accuracy. For instance CCSD(T) calculations are often performed on geometries optimized at B3LYP level of calculation. Binding energies calculated with gradient-corrected functionals are only weakly dependent on the method used for geometry optimization. The approach of using low-level structures (i.e. LDA) coupled with higher level single-point energies has often been found to reduce computational time by 75% with no loss in accuracy of the computed binding energies **[49,57**]. It is now well established that LDA provides geometries rather close to crystal XRD, whereas GGAs give slightly larger distances, excepted for bonds linking (covalently) H atom. Most important is the fact that the distance shifts between isomers bonds are very similar, whatever the retained XC functional is.

Solvation effect was also estimated, through the COSMO model **[50]**. The energy decomposition analysis **[51**,**52**,**53**,**54]** was performed to provide the respective contributions

of the three fragments constituting the complexes, namely the acetylcholine/choline cations (ACh^+/Ch^+), the cavitand (**1**), and the picrate counterion (Pic^-).

4. Results and Discussion

Figure 2A and 2B present mass spectra obtained from the solutions (A) and (B), respectively. The insets exhibit the 80-200 amu range indicative of the presence of the Ch^+ and/or the ACh^+ ions. The mass spectrum of the solution (A) shows a dominant peak located at m/z 1375 amu attributed unambiguously to the Ch^+-**1** complex ion, in addition to the Ch^+ ions observed at m/z 104 amu (Fig 2A). Both type of ions are expected to be present in the solution (A) in which the choline ions are in excess number in respect to that of the host molecules. The mass spectrum presented in Figure 2B is obtained from the solution (B). It shows two extra features appearing at m/z 146 amu and 1417 amu. These are assessed to the ACh^+ ion and the ACh^+-**1** ion respectively. Since the solution (B) is prepared from the solution (A), this result provides clear evidence for the strong potentiality of the acetylcholine ions to substitute the choline ions within in the Ch^+-**1** ion complex. In other words, the present mass spectrometry results are in good agreement with the observations from analysis of solutions that have found the preferential trapping of the ACh^+ ions to the detriment of the Ch^+ ions by the parent phosphonato cavitand **1** host, as it has been previously observed for the phosphonato cavitand **2** bearing C_{11}-alkyl chains at the narrow rim (Fig.1) **[8]**.

The breakdown or survival curves resulting from the dissociation of the Ch^+-**1** and the ACh^+-**1** ion complexes induced by collisions with the Ar targets are presented in Figure 3A and 3B respectively. As it can be seen, the disappearance of the ion complexes leads only to the production of the Ch^+ or ACh^+ ion species. No other ion fragments can be observed indicative that the collisions do not promote more complex reactions such as modifications of the cavitand in the ion-**1** complex as it can be seen in some CID of experiments **[55]**. On the

other hands, it is not known whether at high collision energies in the present experiments, the production of the Ch^+ or ACh^+ can arise concomitantly with the dissociation of the cavitand into neutrals species. Nevertheless, at the threshold collision voltage, the dissociation of the ion complex results essentially in the expulsion of the choline or the acetylcholine ion from the ion complexes. Thus the threshold energy is estimated in the laboratory frame to 48 eV for the fragmentation of the ACh^+-**1** ion complex ($E_{th}^{LAB}(ACh^+) = 48$ eV) and 51.5 eV for that of the Ch^+-**1** ion system ($E_{th}^{LAB}(Ch^+) = 51.5$ eV). These thresholds can be converted to the center-of-mass coordinated to $E_{th}^{CM}(ACh^+) = 1.181$ eV and $E_{th}^{CM}(Ch^+) = 1.315$eV, respectively. Indeed, the fraction of the laboratory translational energy, E^{LAB}, that is available for inelastic scattering is the energy of the collision in the center of mass of the colliding partner, $E^{CM} = (E^{LAB}-E^{LAB}_o).[m_2/(m_1+m_2)]$, m_1 and m_2 being the mass of the incident and the target, respectively, and E^{LAB}_o the reference energy (5eV) **[38,56]**. Thus it is clear that: 1) in the gas phase CID experiments the acetylcholine ion is less strongly bound than the choline to the cavitand, 2) mass spectrometry measurements indicate that the acetylcholine-cavitand complex is promoted over the choline-cavitand as observed in solution. This observation has been previously reported for the selective capture of these ammonium guests by the cavitand host **2** for which the exchange constant has been measured **[8]**. Furthermore the CID results from the ions complexed with **2** (Supplementary Information SI-1) also show that $E_{th}(Ch^+) > E_{th}(ACh^+)$.

Calculations were performed for complexes in the presence (i.e., Ch^+-**1**-Pic^- or ACh^+-**1**-Pic^-) as well as in the absence of the picrate counterion (i.e., Ch^+-**1** or ACh^+-**1**). As already said, to save computational time, geometries of the complexes were optimized at LDA level since the method provides already reasonable configurations [**46**,**49**,**57**,**58**,**59**]**.** Thus the optimized geometries of the neutral complexes were found rather close to that obtained by X-

Ray diffraction **[8]**, the picrate counterion contributing to keep the benzyl groups parallel as shown in Fig. 4. The benzyl groups are separated from 7.19Å, the planar picrate ion lying in between them. When the picrate counterion is detached, the benzyl groups relax toward a more "open" structure. The latter releases some constrain on the opposite side of the cavitand, allowing a stronger interaction with the acetylcholine/choline ion (Fig. 5). The distance between the acetylcholine or choline cation (measured from the N position) to the PO groups (measured from the O=P position, i.e. the N···OP distances) remains almost unchanged through the relaxation process. However the distance between the acetylcholine and the choline cation (measured from the N position) to the two OH groups (measured from the O positions, i.e., N···OH) increases by ca 0.2 Å for the former through the relaxation process whereas the distance between the choline cation to the two OH groups but decreases by ca 0.2 Å for the latter. Therefore in the absence of the picrate counterion, the complexation of the choline becomes stronger through an increased interaction between one OH group and the choline cation (Table I). Thus the difference in the complexation of the acetylcholine and the choline cation with cavitand **1** can be supported by the difference in the steric or the electrostatic interactions due to the presence or absence of a carbonyl group in the guest structure.

The Mulliken charges show a clear repartition of the charges, with a positive +1 (0.89) charge on the choline cation and a negative -1 (-1.01) charge of the picrate counterion. Therefore **1** remains quasi neutral in the complex (0.12). Such charge distribution allows an energy decomposition analysis between fragments clearly characterized by their (integer) charge (+1, 0,-1) and their geometries (the atom positions within the complex), as discussed in the following.

The bonding energies reported in Table 2 are obtained from the LDA calculations. In ADF, energies, called bonding energies, are calculated directly (in the same numerical

integration grid), with respect to the fragments, by one single numerical integral of the difference energy density between the overall molecule and the constituting fragments. These energies are calculated with respect to reference energies, which are, in general, spherical restricted (no spin) atoms. In the present work, the reported bonding energies are calculated with respect to the three fragments constituting the complex, i.e., the picrate counterion, the cavitand and the acetylcholine or the choline cation. More precisely, the three fragments, namely the picrate (negative) ion, the choline cation, and the cavitand have been calculated in their geometry within the complex, and the energy of the complex has been calculated, -and analyzed-, with respect to these three fragments. The geometry optimization of the complex was performed in a first step, providing bonding energies with respect to spherical atoms, as usual. Following Bickelhaupt and Baerends analysis scheme **[51]** the bonding energies can be separated into different contributions (Table 2). The binding energies of the ion-pairs, i.e., ACh^{+}-Pic^{-} and Ch^{+}-Pic^{-} are found to be very close, 1.68eV and 1.63eV, respect., They are dominated by the electrostatic interaction between the two ions as it could be anticipated. However, these values are significantly weaker than the interaction of the cation or the anion with the cavitand to form a charged complex: ACh^{+}**-1**, Ch^{+}**-1** or Pic^{-}**-1**. It is nevertheless noteworthy that the acetylcholine cation interacts more strongly (ca. 4.08eV) with the cavitand than the choline ion (3.66eV). The origin resides in part on the enhancement of the electrostatic contribution between the acetylcholine cation and the cavitand, in other words, localized on the acetyl group, and in part on a subtle balance of the kinetic, steric, orbital interactions and exchange-correlation energy contributions; all these terms increase with the number of atoms, i.e. of the electronic density, as expected.

Whereas LDA calculations are known to provide reasonable geometries of complexes, the energies are definitely poor in the chemical accuracy for the comparison of the stability of isomers and to calculate reaction energies and barrier energies **[54**,**59]**. Therefore we have

performed post-SCF calculations of our complexes at geometries optimized at LDA level using electronic densities (i.e. orbitals) calculated at GGA level (PBE functional). Among the 65 different combinations of exchange and correlation functionals available in the ADF code, we have retained 15 most relevant functionals (1 LDA, 5 GGAs, 2 metaGGAs, 4 hybrids, 3 dispersion-corrected functionals). The calculated energies are reported in the following Tables 4a and 4b. Table 4c provides the differences in the interaction energies between the acetylcholine and the choline complexes. Although the absolute value for the energies differs, the conclusion remains the same: ACh^{+}-**1** is more stable than Ch^{+}-**1** by 0.076 eV. It is also observed the ACh^{+}-**1**-Pic^{-} complex is more bound than the choline substituted complex by 0.031 eV. This correlates well with the larger dipole value of the acetylcholine complex (38.25 Debye) with respect to the choline complex (28.37 Debye). The averages obtained from the 65 functional combinations available in the ADF2012 version (Table 4c) do not show significant variations. It is obvious that such an average is dependent to the arbitrary choice of the retained functionals (65 in the 2012 release of ADF), although it becomes more and more meaningful as far as the number of functionals increases. A careful elimination of a few functionals from the panel, namely the LDA and a few "exotic" combinations **[60]** would probably lead to quasi similar averages, but with a reduced spread among them. Tables of the data for the 65 functionals are given in Supplementary information. Interestingly, the total bonding energies of the complexes are found to be almost equal to the sum of the two-by-two fragment contributions, indicating that three-body interactions between the three fragments (picrate counterion, cavitand and acetylcholine/choline cation) are negligible, at least by two orders of magnitude. This can be checked in Tables 2, 3, 4A and 4B where "total" means a calculation of the whole system, whereas left columns report two by two interactions.

The COSMO model has been used to investigate the potential influence induced by the solvent. It has been seen that the solvation model does not significantly affect the energy

contributions. This is expected since the relatively large size and compact volume of the complex (nearly 200 atoms) tends to prohibit the solvent to penetrate inside the complex that would modify the interaction energies. Therefore, although some contributions are enhanced by the solvation (e.g. electrostatic interaction), the solvation total effect on the energy is very small (Table 3) and does not play a different role on both of the acetylcholine/choline complexes, as compared to the results in Table 2.

We have also investigated the relaxation of the Ch^+-**1**-Pic^- and ACh^+-**1**-Pic^- complexes after losing the negative counterion into Ch^+-**1** and ACh^+-**1** cation complexes, respectively. As seen the results reported in Table 5, it is found that after relaxation the ACh^+-**1** cation becomes less stable than the Ch^+-**1** species by 0.2eV at all levels of calculation (GGA, metaGGA, hybrid functionals), excepted at the LDA level (opposite sign). In case of dispersion-corrected functionals, no significant numbers are obtained. The relative stability of the Ch^+-**1** and the ACh^+-**1** complexes can also be estimated by comparing the variation of the bonding energies between the acetylcholine/choline cations and the cavitand fragment (Table 6). It is shown that the relaxation of the Ch^+-**1** cation yields at least 0.227eV stabilization energy arising from some spatial rearrangement. In contrast the formation of the ACh^+-**1** cation complex does not lead to a significant inter-molecular rearrangement with thus substantial stabilization energy. This structural change may be assigned to the decrease of some strain within the complex when the counterion is released. The picrate counterion forces two phenyl groups to lie parallel, and consequently reduces the possibility of P=O or OH groups to strongly interact with the choline cation. In this particular case, whereas the three P=O groups and one OH group remain at the same place in presence or in absence of picrate, the second OH may come much closer to the choline than to the acetylcholine. Thus the stabilization of the Ch^+-**1** cation overshoots the relative smaller stability of the Ch^+-**1**-Pic^-, with respect to the ACh^+-**1** (0.05-0.20eV).

From these above analyses, it is likely that for the solution (A) the Ch^+Pic^- salt may dissociate to form the Ch^+-**1** or Pic^--**1** ions. Alternatively the Ch^+-**1**-Pic^- complex can be also directly formed in the solution. This neutral complex may further detach the picrate counter ion at the needle region of the ESI on which +3000V is applied, considering the relatively weak interaction between **1** and Pic^-. *In fine* it is the Ch^+-**1** ions that are observed by the ESI in the positive mode (Fig. 2). For the solution (B), the added ACh^+ ions surrogate the choline ions within the complexes to form ACh^+-**1** or ACh^+-**1**-Pic^-. In fact the direct replacement of the choline ion in the Ch^+-**1** is not favored according to the energetic arguments shown above (Table 5). In contrast the substitution of acetylcholine cation within the neutral Ch^+-**1**-Pic^- complex is energetically more advantageous (Tables 4). Similarly to previously, the weakly picrate anion detaches from the neutral ACh^+-**1**-Pic^- complex in the needle region of the ESI to produce the ACh^+-**1** ions. Therefore the preferential capture already observed previously by mass spectrometry **[8]** consists to the substitution of the Ch^+ choline ion by the ACh^+ within the neutral Ch^+-**1**-Pic^- complex. Once the Ch^+-**1** or the ACh^+-**1** complexes are formed, they relax to their geometry for which the binding energy is stronger for the former cation complex in agreement with the results shown in figure 3.

In the CID experiments, during the journey in the collision cell the complex ion experience multiple collision events prior to breakup **[61,62,63,64]**. Such a dissociation method can be referred as a slow heating of the investigated system since the precursor ions are gradually vibrationally and rotationally excited **[65]**. Thus the threshold voltage dissociation can reflect the energy requires to dissociate the ion complex or to overcome the binding of the ion to the neutral cavitand. Since the measurements have been undertaken with the same experimental conditions (e.g., collision gas pressure), it is likely that both the ACh^+-**1** and the Ch^+-**1** ion complexes experience the same average of collision number. Assuming furthermore a same amount of energy deposited in each ion complex per collision, the

estimate value of $E_{the}^{CM}(ACh^+)/E_{th}^{CM}(Ch^+)$ = 0.9 can be reasonably well compared to the ratio of the binding energies in Table 5 (0.85). It is noteworthy that the calculations have been performed for the fundamental state of the ion complex, which could slightly differ within the experimental conditions.

5. Conclusions

In this work we investigate the processes by which the molecular recognition operates through the example of the ACh^+-**1** and Ch^+-**1** systems. From the above analysis the substitution of the choline ion by the acetylcholine ion in the solution must arise from the Ch^+-**1**-Pic^- complex rather than the Ch^+-**1**. As shown by the DFT calculations, this surrogacy process is an energy controlled mechanism. Indeed since the 'cation-**1**-counterion' complex is more stable than the 'cation-**1**' system, it is likely that the former structure is predominantly present in the solution. The observation of the 'cation-**1**' complexes by mass spectrometry is directly related to the ionization process. For the ESI the electric field present in the needle region is sufficient to expulse the picrate counterion from the neutral complex because of the weak interaction energy between the picrate anion and the *3i*PO cavitand. The 'cation-**1**' then relaxes to their equilibrium state for which Ch^+-**1** is more strongly bound than ACh^+-**1** as observed by CID experiments. Thus extrapolating the physical-chemistry data (e.g., binding energies) obtained from the gas phase measurements to those in the solution is often not a straightforward step but the relative stability and exchange constants can be accessible by ESI measurements.

6. Acknowledgments

This work has been supported by the French *Agence Nationale de la Recherche* through grants n° ANR-06-BLAN-0319 and ANR-06-BLAN-0411 (HAC, BF and MF) and the GENCI/CINES for HPC resources/computer time through Project cpt2130 (HC).

FIGURE 1

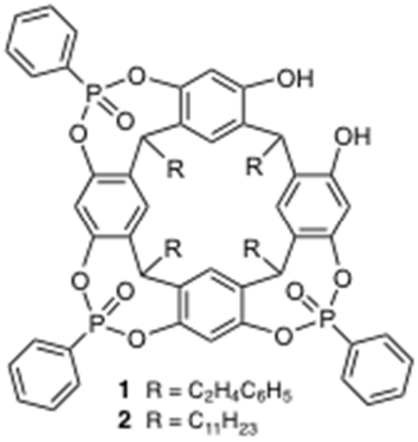

FIGURE 2

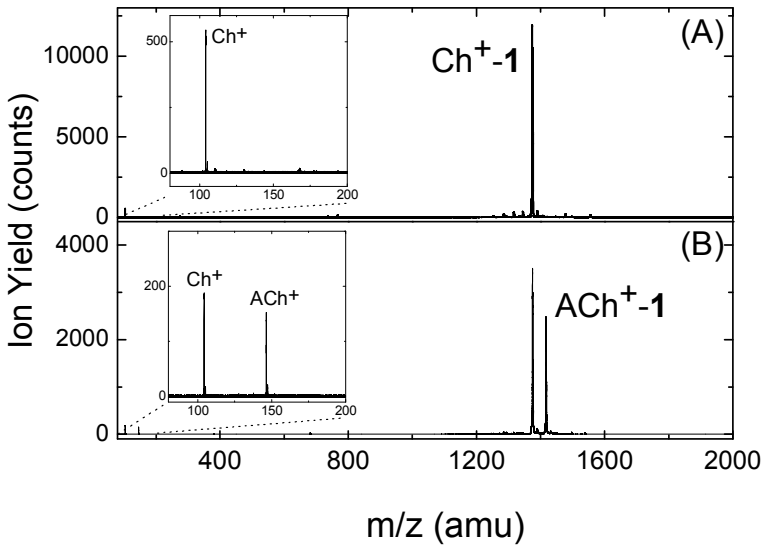
(A)
Ch+-1
Ch+
(B)
ACh+-1
Ch+
ACh+
Ion Yield (counts)
m/z (amu)
0
5000
10000
2000
4000
400
800
1200
1600
2000
100
150
200
500
200

FIGURE 3

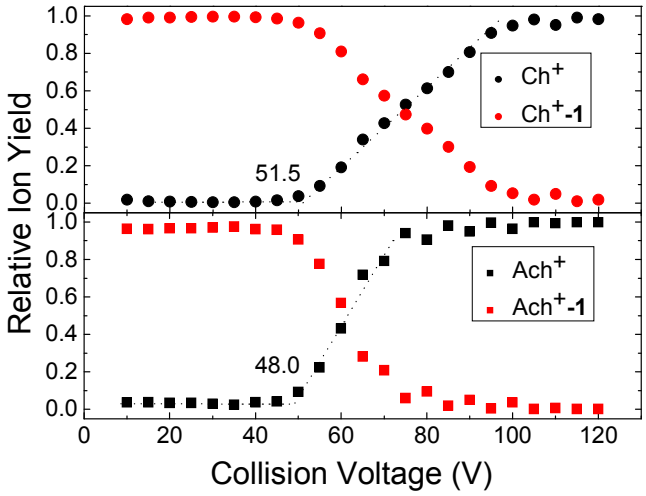
Relative Ion Yield
Collision Voltage (V)
Ch+
Ch+-1
51.5
Ach+
Ach+-1
48.0
0.0
0.2
0.4
0.6
0.8
1.0
0
20
40
60
80
100
120

FIGURE 4

A

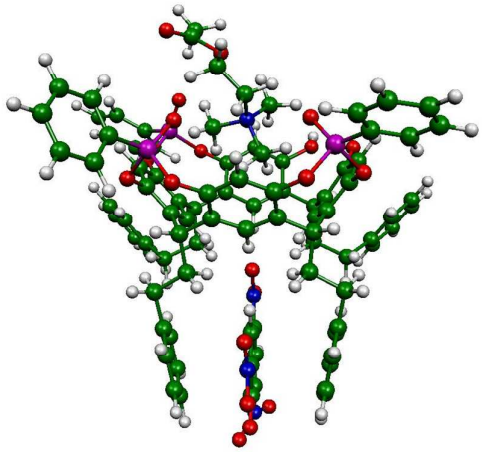

B

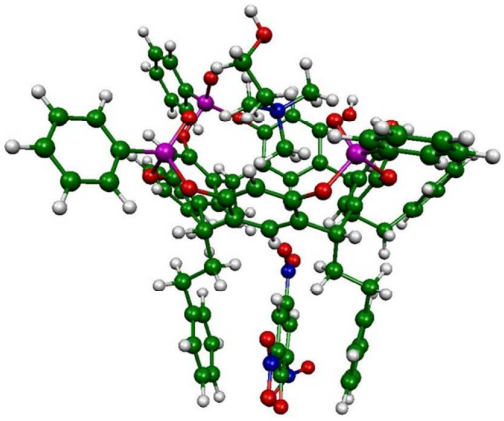

FIGURE 5

A

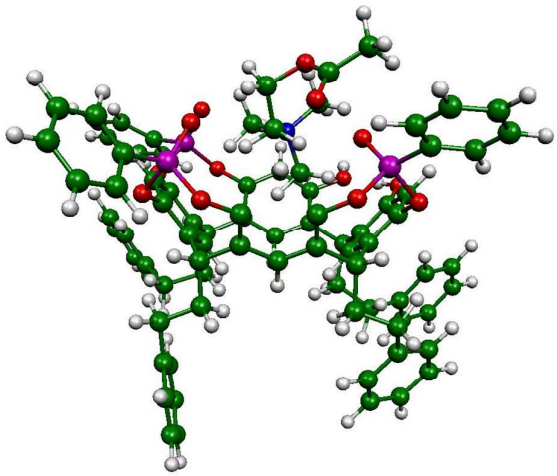

B

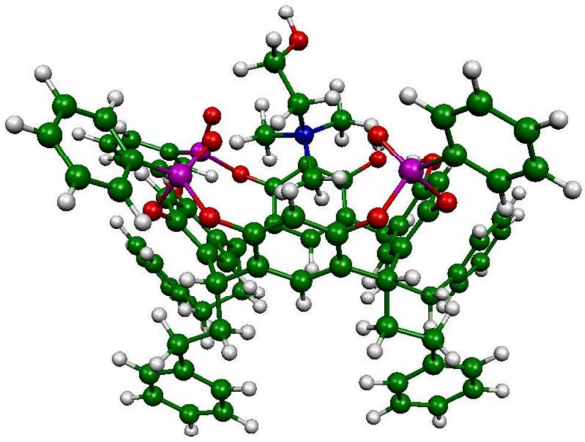

TABLE 1

	Acetylcholine-**1** complex **with** Pic^- counterion	Acetylcholine-**1** 3iPO complex **without** Pic^- counterion	Choline-**1** complex **with** Pic^- counterion	Choline-**1** complex **without** Pic^- counterion
Distances between the benzyl inserting the picrate counterion	7.198 Å between phenyl barycenters (5.68 – 6.74) Å range between analog C	7.953 Å between phenyl barycenters (6.93 – 9.04) Å range between analog C	7.194 Å between phenyl barycenters (5.65 – 6.76) Å range between analog C	8.047 Å between phenyl barycenters (5.60 – 10.49) Å range between analog C
N…O distances between the choline N^+ and the three O=P	4.202, 3.502, 3.448 (average: 3.83)	4.152, 4.056, 3.162 (average: 3.79)	4.215, 3.667, 3.365 (average: 3.74)	4.323, 3.478, 3.375 (average: 3.72)
N…O distances between the choline N^+ and the two O-H	4.969, 4.933 (average: 4.95)	5.181, 5.102 (average: 5.14)	5.001, 4.770 (average: 4.89)	4.784, 4.720 (average: 4.75)

TABLE 2

Acetylcholine complex				
Interactions:	Ach^+-**1**	Pic^--**1**	Ach^+-Pic^-	total
Energy contributions:				
Electrostatic	-3.79	-3.97	-1.61	-9.36
Kinetic	-7.26	-11.90	0.16	-18.99
Coulomb (Steric+OrbInt)	12.31	18.88	-0.27	30.92
XC Energy	-5.35	-6.17	0.03	-11.48
Total	-4.08	-3.15	-1.68	-8.91
Choline complex				
Interactions:	Ch^+-**1**	Pic^--**1**	Ch^+-Pic^-	total
Energy contributions:				
Electrostatic	-3.32	-3.88	-1.57	-8.77
Kinetic	-6.36	-12.08	0.29	-18.16
Coulomb (Steric+OrbInt)	10.71	18.80	-0.37	29.14
XC Energy	-4.68	-6.00	0.03	-10.65
Total	-3.66	-3.15	-1.63	-8.44
Differences Ch - ACh - complexes				
Interactions:	[Ch^+-**1**] – [ACh^+-**1**]	[Pic^--**1**] – [Pic^--**1**]	[Ch^+-Pic^-] – [ACh^+-Pic^-]	total
Energy contributions:				
Electrostatic	0.46	0.09	0.04	-0.59
Kinetic	0.89	-0.18	0.12	0.84
Coulomb (Steric+OrbInt)	-1.60	-0.08	-0.10	-1.78
XC Energy	0.67	0.17	-0.01	0.83
Total	0.43	-0.01	0.06	0.48

TABLE 3

ACh complex				
Interactions:	ACh^+-**1**	Pic^--**1**	ACh^+- Pic^-	total
Energy contributions:				
Electrostatic	-5.08	-4.09	-1.62	-10.79
Kinetic	-4.14	-9.65	0.04	-13.75
Coulomb (Steric+OrbInt)	9.10	16.74	-0.08	25.76
XC Energy	-4.50	-6.13	0.01	-10.61
Solvation	-3.18	-5.07	5.09	-3.17
Total	-7.79	-8.21	3.44	-12.56
Ch complex				
Interactions:	Ch^+-**1**	Pic^--**1**	Ch^+- Pic^-	total
Energy contributions:				
Electrostatic	-4.43	-4.01	-1.56	-9.99
Kinetic	-3.96	-9.75	0.02	-13.69
Coulomb (Steric+OrbInt)	8.24	16.59	-0.07	24.75
XC Energy	-3.95	-5.97	0.02	-9.90
Solvation	-3.20	-5.11	5.06	-3.24
Total	-7.30	-8.24	3.47	-12.07
Differences Ch - ACh complexes				
Interactions:	(A)Ch^+-**1**	Pic^--**1**	(A)Ch^+- Pic^-	total
Energy contributions:				
Electrostatic	0.65	0.09	0.06	0.79
Kinetic	0.18	-0.10	-0.02	0.06
Coulomb (Steric+OrbInt)	-0.86	-0.15	0.01	-1.01
XC Energy	0.55	0.16	0.01	0.71
Solvation	-0.02	-0.03	-0.02	-0.07
Total	0.49	-0.04	0.03	0.49

TABLE 4A

Interactions:	Ref	Ch^+-**1**	Pic^--**1**	Ch^+-Pic^-	total
XC Energy Functional					
LDA (VWN)	[45]	**-2.491**	**-1.360**	**-1.644**	**-5.496**
PW91	[66]	-1.377	0.185	-1.646	-2.838
BLYP	[67,68]	-0.794	0.970	-1.644	-1.468
BP86	[69]	-1.082	0.594	-1.645	-2.133
PBE	[48]	**-1.333**	**0.258**	**-1.646**	**-2.720**
RPBE	[70]	-0.654	1.189	-1.647	-1.112
BmTau1	[71]	0.048	2.163	-1.645	0.567
TPSS	[72]	-1.132	0.506	-1.645	-2.270
PBE-D	[73]	4.220	5.187	-7.637	1.771
TPSS-D	[68,69]	6.273	7.078	-9.633	3.718
TPSSh	[68]	-1.208	0.423	-1.644	-2.429
B3LYP	[74,63,64]	**-1.084**	**0.614**	**-1.641**	**-2.111**
PBE0	[75]	-1.485	0.098	-1.643	-3.030
M06	[76]	-2.204	-0.909	-1.645	-4.757
B3LYP-D	[70,69]	6.691	7.514	-10.029	4.177
Averages:					
GGA		-1.05	0.64	-1.65	-2.05
metaGGA		-0.54	1.34	-1.65	-0.85
hybrids		-1.50	0.06	-1.64	-3.08

TABLE 4B

Interactions:	ACh^+-**1**	Pic^--**1**	ACh^+- Pic^-	total
XC Energy Functional				
LDA (VWN)	**-2.755**	**-1.311**	**-1.688**	**-5.754**
PW91	-1.509	0.262	-1.688	-2.936
BLYP	-0.878	1.057	-1.686	-1.507
BP86	-1.187	0.672	-1.687	-2.202
PBE	**-1.453**	**0.337**	**-1.688**	**-2.804**
RPBE	-0.702	1.285	-1.689	-1.107
BmTau1	0.046	2.273	-1.688	0.631
TPSS	-1.230	0.585	-1.687	-2.332
PBE-D	4.190	5.267	-7.689	1.768
TPSS-D	6.294	7.159	-9.688	3.764
TPSSh	-1.313	0.501	-1.685	-2.497
B3LYP	**-1.191**	**0.698**	**-1.684**	**-2.177**
PBE0	-1.615	0.174	-1.684	-3.126
M06	-2.399	-0.816	-1.711	-4.926
B3LYP-D	6.709	7.600	-10.085	4.224
Averages:				
GGA	-1.15	0.72	-1.69	-2.11
metaGGA	-0.59	1.43	-1.69	-0.85
hybrids	-1.63	0.14	-1.69	-3.18

TABLE 4C

Interactions:	[Ch^+-**1**] - [ACh^+-**1**]	[Pic^--**1**] - [Pic^--**1**]	[Ch^+- Pic^-] - [ACh^+- Pic^-]	[Ch^+-**1**- Pic^-] – [ACh^+-**1**- Pic^-]
XC Energy Functional				
LDA (VWN)	**0.26**	**-0.05**	**0.04**	**0.26**
PW91	0.13	-0.08	0.04	0.10
BLYP	0.08	-0.09	0.04	0.04
BP86	0.10	-0.08	0.04	0.07
PBE	**0.12**	**-0.08**	**0.04**	**0.08**
RPBE	0.05	-0.10	0.04	-0.01
BmTau1	0.00	-0.11	0.04	-0.06
TPSS	0.10	-0.08	0.04	0.06
PBE-D	0.03	-0.08	0.05	0.00
TPSS-D	-0.02	-0.08	0.06	-0.05
TPSSh	0.10	-0.08	0.04	0.07
B3LYP	**0.11**	**-0.08**	**0.04**	**0.07**
PBE0	0.13	-0.08	0.04	0.10
M06	0.20	-0.09	0.07	0.17
B3LYP-D	-0.02	-0.09	0.06	-0.05
Averages:				
GGA	0.10	-0.08	0.04	0.06
metaGGA	0.05	-0.09	0.04	0.00
hybrids	0.13	-0.08	0.05	0.10
65 functionals	0.066	-0.087	0.043	0.022
all functionals excluding dispersion-corrected ones	0.076	-0.087	0.042	0.031

TABLE 5

Interactions:	[Ch-**1**]$^+$	[ACh-**1**]$^+$	[Ch-**1**]$^+$ - [ACh-**1**]$^+$
XC Energy Functional:			
LDA (VWN)	-2.59	-2.83	0.23
PW91	-1.57	-1.48	-0.09
BLYP	-1.03	-0.79	-0.24
BP86	-1.28	-1.12	-0.16
PBE	**-1.53**	**-1.42**	**-0.11**
RPBE	-0.90	-0.60	-0.30
BmTau1	-0.27	0.22	-0.49
TPSS	-1.33	-1.18	-0.15
PBE-D	4.41	4.38	0.03
TPSS-D	6.59	6.55	0.04
TPSSh	-1.41	-1.28	-0.13
B3LYP	**-1.31**	**-1.14**	**-0.17**
PBE0	-1.68	-1.61	-0.07
M06	-2.41	-2.53	0.13
B3LYP-D	7.00	6.98	0.02
Averages:			
GGA	-1.26	-1.08	-0.18
metaGGA	-0.80	-0.48	-0.32
hybrids	-1.70	-1.64	-0.06
65 functionals	-0.52	-0.34	-0.18
all functionals excluding dispersion-corrected ones	-1.28	-1.08	-0.20

TABLE 6

Free cation interaction energy - interaction energy within the complex including the picrate counterion.		
	Interactions:	
	[Ch-**1**]$^+$	[ACh-**1**]$^+$
XC Energy Functional:		
LDA (VWN)	0.102	0.073
PW91	0.193	-0.033
BLYP	0.236	-0.091
BP86	0.197	-0.070
PBE	**0.196**	**-0.036**
RPBE	0.251	-0.101
BmTau1	0.314	-0.178
TPSS	0.197	-0.047
PBE-D	-0.191	-0.195
TPSS-D	-0.319	-0.259
TPSSh	0.198	-0.034
B3LYP	**0.230**	**-0.047**
PBE0	0.198	-0.005
M06	0.205	0.136
B3LYP-D	-0.312	-0.270
Averages:		
GGA	0.215	-0.066
metaGGA	0.255	-0.112
hybrids	0.208	0.012
65 functionals	0.182	-0.062
all functionals excluding dispersion- corrected ones (and VS98)	0.227	-0.029

LIST of TABLES

TABLE 5. Differences in interaction energy between fragments of choline Ch and acetylcholine ACh complexes with cavitand **1** in the relaxed geometry of the cation. Bonding energies (eV) of the fragments from densities calculated at GGA level and all electron TZP basis set. A positive value indicates a higher stability of the ACh complex with respect to the Ch complex. (bold lines refer to the most widely used functionals, **-D** functionals are dispersion-corrected functionals)

TABLE 6. Differences in interaction energy between fragments of choline Ch and acetylcholine ACh complexes with **1** in their two (within the neutral complexes with the picrate counterion, and in the relaxed geometry of the (acetyl)choline - **1** cations. Bonding energies (eV) of the fragments from densities calculated at GGA level and all electron TZP basis set. A positive value indicates a higher stability in the free ACh/Ch - **1** cation with respect to the neutral ACh/Ch complex with the picrate counterion. (bold lines refer to the most widely used functionals, **-D** functionals are dispersion-corrected functionals)

FIGURE CAPTIONS

FIGURE 1. Structure of the *3iPO* phosphonato cavitands **1** and **2.** The label 1 and 2 correspond to R=$C_2H_4C_6H_5$ and R=$C_{11}H_{23}$, respectively. In the present work we investigate the **1** host.

FIGURE 2. Mass spectra a solution of **1**-Ch^+Pic^- in which a solution of ACh^+Pic^- of a volume of (A) (0μL), (B) (5 μL) has been added. The insets display the 80-200 amu range.

FIGURE 3. Survival (or breakdown) curves result from the dissociation of (**1**-Ch^+) and (**1**-ACh^+) induced by collisions on Ar targets. The voltage threshold for the appearance of the Ch^+ and the ACh^+ is 51.5V and 48.0V respectively. The dashed lines are guides-to-the-eye.

FIGURE 4. Calculated structure of the (A) Ch^+-**1**-Pic^- and (B) ACh^+-**1**-Pic^- complex.

FIGURE 5. Calculated structure of the relaxed (A) Ch^+-**1** and (B) ACh^+-**1** complex after removing the picrate counterion.

REFERENCES

1 L.M. Salonen, M. Ellerman, F. Diederich, *Angew. Chem. Int. Ed.* **50** 4808 (2011).

2 M.C. An, W. Lin, J. Yang, B. Dominguez, D. Padgett, Y. Sugiura, P. Aryal, T.W. Gould, R.W. Oppenheim, M.E. Hester, B.K. Kaspar, C.-P. Ko, K.F. Lee, *PNAS* **107** 10702 (2010).

3 H. Yang, S. Kunes *PNAS* **42** 15213 (2004).

4 M. Harel, D. M. Quinn, H. K. Nair, I. Silman, J. L. Susman, *J. Am. Chem. Soc.* **118** 2340 (1996).

5 D. A. Dougherty *Science* **271** 163 (1996).

6 N. Zacharias, D. A. Dougherty, *Trends Pharmacol. Sci.* **23** 281 (2002).

7 E. Kalenius, D. Moiani, E. Delcanale, P. Vainiotalo *Chem. Comm* 3865 (2007).

8 H. Abdoul-Carime, M.M. Harb, C.G. Montano, C. Teyssier, B. Farizon, M. Farizon, J. Vachon, S. Harthrong, J.-P. Dutasta, E. Jeanneau, T.D. Mark, *Chem Phys Lett* **513** 82 (2012).

9 S. Roelens, R. Torriti, *J. Am. Chem. Soc.* **120** 12443 (1998).

10 S. Bartoli, S. Roelens, *J. Am. Chem. Soc.* **124** 8307 (2002).

11 P. Sarri, F. Venturi, F. Cuda, S. Roelens, *J. Org. Chem.* **69** 3654 (2004).

12 A. Arduini, A. Pochini, A. Secchi, *Eur. J. Org. Chem.* 2325 (2000).

13 K. Murayama, K. Aoki, *Chem. Commun.* 119 (1997).

14 H. Mansikkamäki, M. Nissinen, C. Schalley, K. Rissanen, *New J. Chem.* **27** 88 (2003).

15 N. K. Beyeh, D. P. Weimann, L. Kaufmann, C. A. Schalley, K. Rissanen, *Chem. Eur. J.* **18** 5552 (2012).

16 L. Garel, B. Lozach, J.-P. Dutasta, A. Collet, *J. Am. Chem. Soc.* **115** 11652 (1993).

17 C. Garcia, D. Humiliere, N. Riva, A. Collet, J.-P. Dutasta, *Org. Biomol. Chem.* **1** 2207 (2003).

18 T. Brotin, J.-P. Dutasta, *Chem. Rev.* **109** 88 (2009).

19 B.W. Purse, J.Rebek Jr. *PNAS* **102** 10777 (2005).

20 A. Pramanik, D.R. Powell, B.M. Wong, M.A. Hossain, Inorg. Chem. **51** 4274 (2012).

21 M. Isiklan, M.A. Saeed, A. Pramanik, B.M. Wong, F.R. Fronczek, M.A. Hossain, Crystal Growth & Design, **11** 959 (2011).

22 J. Vachon, S. Harthong, E. Jeanneau, C. Aronica, N. Vanthuyne, C. Roussel, J.-P. Dutasta, *Org. Biomol. Chem.* **9** 5086 (2011).

23 J. Vachon, S. Harthong, B. Dubessy, J.-P. Dutasta, N. Vanthuyne, C. Roussel, J.-V. Naubron, *Tet. Asymm.* **21** 1534 (2010).

24 R. M. Yebeutchou, E. Dalcanale, *J. Am. Chem. Soc.* **131** 2452 (2009).

25 R. Pinalli, E. Dalcanale, *Acc. Chem. Res.* **46** 399 (2013).

26 B. Mettra, Y. Bretonnière, J.-C. Mulatier, B. Bibal, B. Tinant, C. Aronica, J.-P. Dutasta, *Supramol. Chem.* **25** 672 (2013).

27 V.B. Di Marco, G.G. Bombi, *Mass Spectrom Rev.* **25** 347 (2006).

28 M. Vincenti, *J. Mass Spectrom* **30** 925 (1995).

29 H. Abdoul-Carime, *J. Chem. Soc, Farad. Trans* **94** 2407 (1998).

30 C. Collette, D. Deharend, E. De Pauw, G. Dive, *J. Am. Soc Mass Spectrom* **12** 304 (2001).

31 M. Meot-Ner, *J Am. Chem. Soc* **105** 4912 (1983).

32 R.B. Sharma, P. Kaberle, *J. Am. Chem. Soc* **106** 3913 (1984).

33 J.S. Bodbelt, C.C. Liou, *Pure Appl. Chem* **65** 409 (1993).

34 C.C. Liou, H.F. Wu, J.S. Brodbelt, *J. Am. Soc Mass Spectrom* **5** 260 (1994).

35 M. Yamashita, J.B. Fenn, *J. Phys. Chem* **88** 4451 (1984).

36 P. Kaberle, AT. Blades M.G. Ikonomou, *Anal Chem* **62** 957 (1990).

37 R. Cole, G. Wang, *Mass Spectrom* **29** 419 (1994).

38 J.A. Laramée, D. Cameron, R.G. Cooks, *J Am Chem Soc* **103** 12 (1981).

39 V. Gabelica, E. De Pauw, *Mass Spectrom Rev* **24** 566 (2005).

40 P.B. Armentrout, *Top Curr Chem* **225** 233 (2003).

41 W. Tian, S.R. Krass, *J. Am. Chem Soc* **130** 10842 (2008).

42 M.H. Amad, N.B. Cech, G.S. Jackson, C.G. Enke, *J Mass Spectrom* **35** 784 (2000).

43 G.W. Collie, G.N. Parkinson, S. Neidle, F. Rosu, E. de Pauw, V. Gabelica, *J. Am. Chem. Soc* **132** 9328 (2010).

44 B. Dubessy, S. Harthong, C. Aronica, D. Bouchu, M. Busi, E. Dalcanale, J.-P. Dutasta, *J. Org. Chem.* **74** 3923 (2009).

45 E. J. Baerends, T. Ziegler, J. Autschbach, D. Bashford, A. Bérces, F. M. Bickelhaupt, C. Bo, P. M. Boerrigter, L. Cavallo, D. P. Chong, L. Deng, R. M. Dickson, D. E. Ellis, M. v. Faassen, L. Fan, T.H.Fischer, C.FonsecaGuerra, A. Ghysels, A. Giammona, S. J. A. van Gisbergen, A. W. Götz, J. A. Groeneveld, O. V. Gritsenko, M. Grüning, S. Gusarov, F. E.Harris, P. van denHoek, C. R. Jacob, H. Jacobsen, L. Jensen, J.W. Kaminski, G. vanKessel, F. Kootstra, A. Kovalenko, M. V. Krykunov, E. van Lenthe, D. A. McCormack, A. Michalak, M. Mitoraj, J. Neugebauer, V. P. Nicu, L. Noodleman, V. P. Osinga, S. Patchkovskii, P. H. T. Philipsen, D. Post, C. C. Pye, W. Ravenek, J. I. Rodrı´guez, P. Ros, P. R. T. Schipper, G. Schreckenbach, J. S. Seldenthuis, M. Seth, J. G. Snijders, M. Solà , M. Swart, D. Swerhone, G. te Velde, P. Vernooijs, L. Versluis, L. Visscher, O. Visser, F. Wang, T. A. Wesolowski, E. M. van Wezenbeek, G. Wiesenekker, S. K. Wolff, T. K. Woo and A. L. Yakovlev, ADF2010, SCM, Amsterdam, 2010.

46 G. te Velde, F. M. Bickelhaupt, E. J. Baerends, C. Fonseca Guerra, S. J. A. van Gisbergen, J. G. Snijders and T. Ziegler, *J. Comput. Chem* **22** 931 (2001).

47 S.H. Vosko, L. Wilk, M. Nusair, *Can. J. Phys*. **58** 1200 (1980).

48 J.P. Perdew, K. Burke, and M. Ernzerhof, *Phys. Rev. Lett.* **77** 3865 (1996), Ibid. E **78** 1396 (1997).

49 N. Zhang, P. Blowers, J. Farrell, *Environmental Science & Technology* **39** 4816 (2005).

50 A. Klamt, *J. Phys. Chem*. **99** 2224 (1995); C.C. Pye and T. Ziegler, *Theor. Chem. Accounts* **101** 396 (1999).

51 K. Kitaura, K. Morokuma, *Int. J. Quant. Chem.* **10** 325 (1976).

52 T. Ziegler and A. Rauk, *Inorg. Chem.* **18** 1755 (1979).

53 T. Ziegler and A. Rauk, *Theor. Chim. Acta* **46** 1 (1977).

54 F.M. Bickelhaupt and E.J. Baerends, *in*: Rev. Comput. Chem.; K. B.Lipkowitz, and D. B.Boyd, Eds.; Wiley-VCH: New York, 2000, Vol. 15, 1-86.

55 T. Gozet, *Int J Mass Spectrom* **279** 113 (2009).

56 D.J. Douglas, *J. Phys. Chem* **86** 185 (1982).

57 H. Chermette, *Coord. Chem. Rev.* **178** 699 (1998).

58 A. C. Scheiner, J. Baker, J. W. Andzelm, *J. Comput. Chem.* **18** 775 (1997).

59 W. Koch, M.C. Holthausen, A Chemist's Guide to Density Functional Theory; Wiley-VCH: Weinheim, 2000.

60 C. Lepetit, H. Chermette, M. Gicquel, J-L. Heully, R. Chauvin, *J. Phys. Chem. A* **111** 136 (2007).

61 K.M. Ervin *Chem.Rev* **101** 391 (2001).

62 S.A. Mc Luckey, J.M. Wells *Chem Rev* **101** 571 (2001).

63 P.B. Armentrout, *J. Chem Phys* **126** 234302 (2007).

64 K. Veykey, *J. Mass Spectrom* **31** 445 (1996).

65 S.A. Mc Luckey, *J Mass Spectrom* **32** 461 (1997).

66 J.P. Perdew in: Electronic Structure of Solids 1991 Ed. P. Ziesche and H. Eschrig (Akademie, Berlin, 1991) p. 11; J.P. Perdew, J.A. Chevary, S.H. Vosko, K.A. Jackson, M.R. Pederson, D.J. Singh, and C. Fiolhais, *Phys. Rev. B* **46** 6671 (1992); Ibid. E **48** 4978 (1993).

67 A.D. Becke, *Phys. Rev. A* **38** 3098 (1988).

68 C. Lee, W. Yang, R.G. Parr, *Phys. Rev. B* 37 785 (1988).

69 J.P. Perdew, *Phys. Rev. B* **33** 8822 (1986); Erratum: J.P. Perdew, *Phys. Rev. B* **34** 7406 (1986).

70 B. Hammer, L.B. Hansen, J.K. Norskov, *Phys. Rev. B* **59** 7413 (1999).

71 E.I. Proynov, H. Chermette, and D.R. Salahub, *J. Chem. Phys.* **113** 10013 (2000).

72 J. Tao, J.P. Perdew, V.N. Starorerov and G.E. Scuseria , *Phys. Rev. Lett.* **91** 146401 (2003); V.N. Starorerov, G.E. Scuseria, J. Tao and J.P. Perdew, *J. Chem. Phys.* **119**12129 (2003).

73 S. Grimme , *J. Comput. Chem.* **27** 1787 (2006).

74 A.D. Becke, *J. Chem. Phys.* **98** 5648 (1993).

75 M. Ernzerhof and G. Scuseria, *J. Chem. Phys.* **110** 5029 (1999); C. Adamo and V. Barone, *J. Chem. Phys.* **110** 6158 (1999).

76 Y. Zhao, D.G. Truhlar, *J. Chem. Phys.* **125** 194101 (2006).